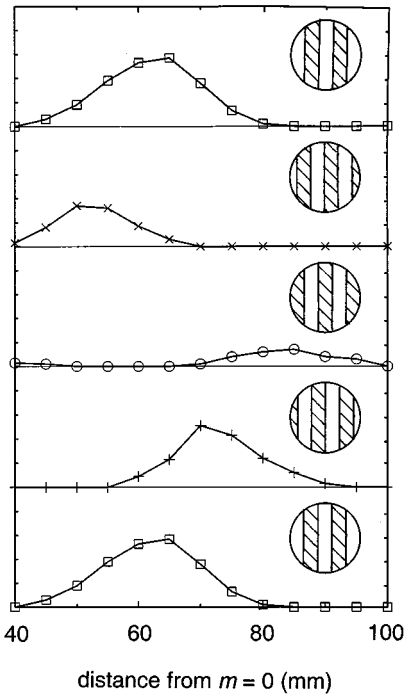

Fig. 4. Scans of the diffraction patterns in the vicinity of $m = -1$ as the shadow pattern is translated across the silicon wafer. The insets show the shadow patterns.

pattern is translated across the silicon wafer. Calculations show this behavior to be expected.

Blurring of the grating edges due to sideways diffusion of the carriers is estimated to be less than 1 mm under the conditions of this experiment.

Similar results were obtained when the silicon was illuminated from the rear. The copper conductor was replaced by a 100 wires per inch nickel mesh. This mesh, with a reflectance of 0.96 at 105 GHz, reflected the millimeter waves, but allowed light to pass through.

In conclusion, the experiments described here have demonstrated that a diffraction grating, produced by projecting a grating pattern onto a semiconductor wafer, can redirect a millimeter-wave beam. The new direction being determined largely by the period of the projected pattern. A measure of fine control over the direction can be achieved by translating the pattern across the wafer.

ACKNOWLEDGMENT

The author would like to thank J. Lizier for his assistance in carrying out the investigation in which the silicon wafer was illuminated from the rear.

REFERENCES

[1] V. A. Manasson, L. S. Savodnik, A. Moussessian, and D. B. Rutledge, "Millimeter-wave diffraction by a photo-induced plasma grating," *IEEE Trans. Microwave Theory Tech.*, vol. 43, pp. 2288–2290, Sept. 1995.

[2] V. A. Manasson, L. S. Sadovnik, P. I. Schnitser, and R. Mino, "Millimeter-wave optically scanning antenna based on photoinduced plasma grating," *Opt. Eng.*, vol. 35, pp. 357–361, 1996.

[3] W. Platte, "LED-induced distributed Bragg reflection microwave filter with fiber-optically controlled change of center frequency in photoconductivity gratings," *IEEE Trans. Microwave Theory Tech.*, vol. 39, pp. 359–363, Feb. 1991.

[4] G. F. Brand, "Diffraction of millimeter waves by projecting a shadow pattern onto a semiconductor," *Int. J. Infrared Millimeter Waves*, vol. 17, pp. 1253–1262, 1996.

[5] P. Lorrain and D. Corson, *Electromagnetic Fields and Waves*, 2nd ed. San Francisco, CA: Freeman, 1970, p. 508 ff.

A Distributed-Feedback Antenna Oscillator

Shin-Lin Wang, Young-Huang Chou, and Shyh-Jong Chung

***Abstract*—In this paper, a new design of the active transmitting antenna array, called the distributed-feedback antenna oscillator, is proposed. The active array is formed by serially connecting several unit cells to a closed loop. Each unit cell contains an amplifier and a two-port antenna, with an overall insertion gain larger than 0 dB and a phase delay equal to a multiple of 360°. The signal traveling on the loop is amplified and radiated in each unit cell. The radiation fields from all the antennas are then combined in free space. A four-element feedback antenna oscillator operating at 10 GHz is demonstrated by using two-port aperture-coupled microstrip antennas. Simulation results show that multiple oscillation modes with different frequencies and different radiation beams may be excited in the antenna oscillator. By experiment, it is found that each oscillation mode can be built by tuning the biases of the oscillator. The measured radiation pattern for each mode agrees very well with the predicted one. For a single-mode operation with a broadside pattern, bandstop filters of a simple geometry are designed and embedded in the oscillator to suppress the unwanted oscillation modes. Finally, the influence of the bias condition on the radiation power of the single-mode oscillator is investigated.**

***Index Terms*—Active antenna, feedback, oscillator, spatial power combining.**

I. INTRODUCTION

Due to the advantages of compact sizes, low weights, and low costs, active transmitting antennas have attracted much attention in the applications of communication and radar systems at the microwave and millimeter-wave frequencies [1]–[3]. By integrating a passive planar antenna with solid-state devices, the active transmitting antenna performs not only as a radiator, but also as an oscillator. The design of an active antenna is essentially that of an oscillator, which could be mainly grouped into two types, i.e., the negative-resistance and feedback types. In the first type, a two-terminal device (IMPATT or Gunn diode) [4] or a three-terminal device [MESFET or high electron-mobility transistor (HEMT)] [5] was first used to create a negative-resistance one-port. The antenna with a suitable input resistance was then connected to the one-port as a radiation load. In the feedback type, a two-port antenna was generated and connected to a pre-designed amplifier [6], [7]. The signal coming from the output of the amplifier was fed to one port of the antenna. With most of the signal power radiated to free space, some of it was coupled out through the second port of the antenna, which was then fed to the amplifier's input. In this design type, the antenna possessed the function of a feedback resonator. To start the oscillation,

Manuscript received February 2, 1999. This work was supported by the Ministry of Education and by the National Science Council, R.O.C., under Contract 89-E-FAO6-2-4.

The authors are with the Department of Communication Engineering, National Chiao Tung University, Hsinchu 300 Taiwan, R.O.C. (e-mail: sjchung@cm.nctu.edu.tw).

Publisher Item Identifier S 0018-9480(00)03754-6.

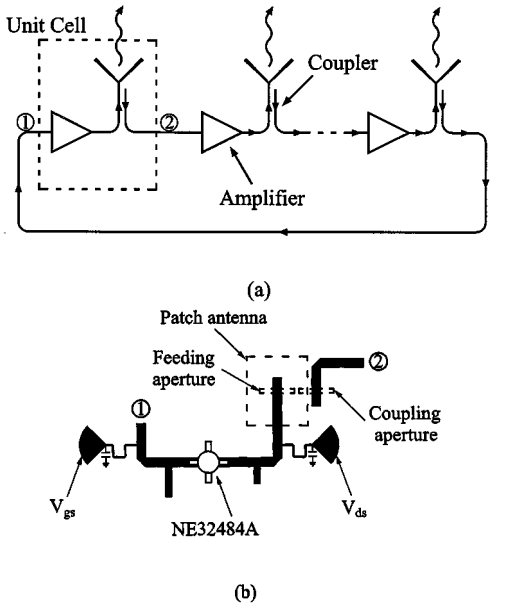

Fig. 1. (a) Conceptual diagram of the distributed feedback antenna oscillator. (b) Circuit layout of a unit cell using the two-port aperture-coupled microstrip antenna.

the closed-loop small-signal gain should be larger than 1–2 dB and the electrical length of the loop should be a multiple of 360°.

By forming several active antennas as an array, the powers radiated from the antennas can spatially combine in free space, resulting in a high output power. This spatial power-combining technique can solve the problems of limited available powers from solid-state devices and high propagation losses in transmission lines, especially for millimeter-wave systems. To stably synchronize the oscillating frequencies of the active antennas, strong injection-locking signals should be applied to the antenna oscillators. These injection signals may come from the mutual couplings between oscillators through an embedded mutual-coupling network [8] or be supplied by an external stable source through a feeding network [9], [10].

In this paper, we propose a new design of active transmitting antennas, called the *distributed-feedback antenna oscillator*, as shown in Fig. 1(a). This design is actually an extension of the feedback-type active antenna, which is formed by serially connecting several unit cells to a closed loop. Each unit cell contains an amplifier and a two-port antenna, with an overall insertion gain larger than 0 dB and a phase delay equal to a multiple of 360°. This structure can be viewed as a strong coupling active antenna array. The signal traveling on the loop is amplified and radiated in each unit cell. The radiation fields from all the antennas are then combined in free space.

II. Design and Simulation

A symmetrical four-element (2 × 2) distributed-feedback antenna oscillator operating at 10 GHz is demonstrated using the unit cell, as shown in Fig. 1(b). The antenna used is a two-port aperture-coupled microstrip antenna [7]. The antenna patches were fabricated on a substrate of $\varepsilon_r = 2.33$ and $h = 31$ mil (thickness) and the amplifier circuits were on a substrate of $\varepsilon_r = 2.2$ and $h = 20$ mil. The signal was fed to the antenna patch through the feeding aperture on the ground plane separating the two substrates and was coupled back to the circuit layer through another aperture under the same patch. The two-port microstrip antenna was designed to be with a transmission loss (due to the radiation of the patch) of 8.5 dB at the center frequency of 10 GHz and a 10-dB return-loss bandwidth of 3.6%. The amplifier designed using an NE32484A HEMT possessed a small-signal gain of about 10 dB at 10 GHz. Note that, by using the two-port aperture-coupled microstrip antennas, no dc block capacitors were needed to isolate the amplifiers' biases. The antenna spacing of the oscillator was set to be 0.6 λ_0 at the design frequency. The whole oscillator was simulated using the harmonic-balance method by the commercial software HP Series IV. In the simulation, the free-space mutual coupling between antennas was neglected.

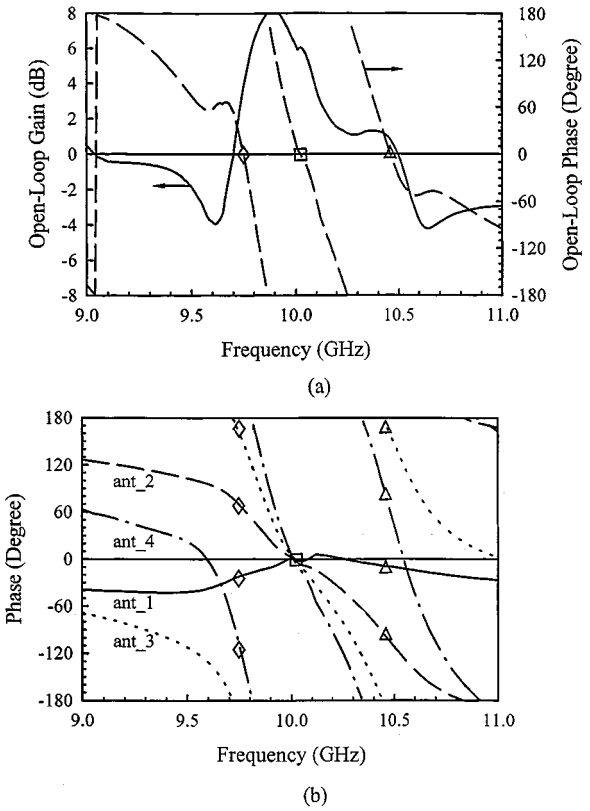

Fig. 2. Simulation results of the four-element antenna oscillator at $V_{\rm ds} = 2$ V and $V_{\rm gs} = -0.3$ V. (a) Open-loop gain and phase as functions of frequency. (b) Antenna signal phases as functions of frequency.

Fig. 2(a) depicts the simulated small-signal open-loop gain and phase as functions of the frequency. The amplifiers' biases were set to be $V_{\rm ds} = 2$ V and $V_{\rm gs} = -0.3$ V. As shown, the loop gain is larger than 0 dB in the frequency band from 9.7 to 10.5 GHz. Within this band, three zero crossing points of the phase curve happen at the frequencies of 9.75, 10.02, and 10.46 GHz, with corresponding loop gains of 3.3, 5.8, and 1 dB, respectively. This means that the circuit may oscillate at these three frequencies since both the gain and phase satisfy the requirements to start the oscillation. It is interesting to look at the signal phases at the four antennas. Simulation results depicted in Fig. 2(b) show that the antennas produce in-phase radiation fields when the circuit oscillates at 10.02 GHz. However, when the oscillation happens at 10.46 GHz (9.75 GHz), a 90° phase delay (advance) occurs between adjacent antennas.

III. Measurement

The designed 2 × 2 feedback oscillator was fabricated and measured. An X-band horn antenna with an HP 8564E spectrum analyzer was used to detect the radiation fields from the antenna array. During measuring, the amplifiers' gate bias ($V_{\rm gs}$) was first fixed at −0.3 V and the drain bias ($V_{\rm ds}$) was then gradually increased from 0 V. As $V_{\rm ds}$ approached 2 V, the active array oscillated at one of the two frequencies

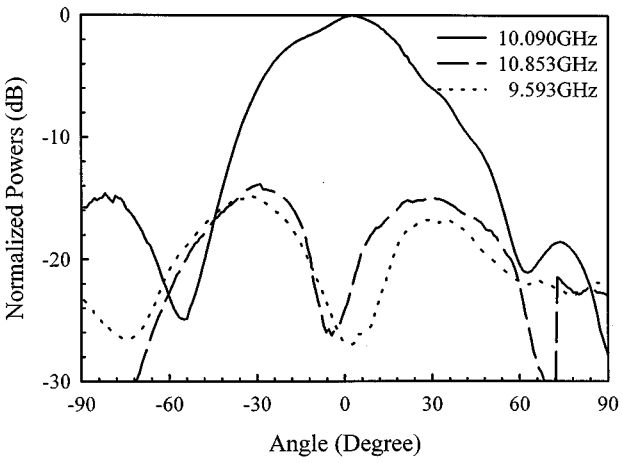

Fig. 3. Measured radiation patterns of the four-element antenna oscillator at the frequencies of 10.090 GHz ($V_{\rm ds} = 3.72$ V), 10.853 GHz ($V_{\rm ds} = 2$ V), and 9.593 GHz ($V_{\rm ds} = 2$ V). The gate bias $V_{\rm gs}$ is fixed at -0.3 V.

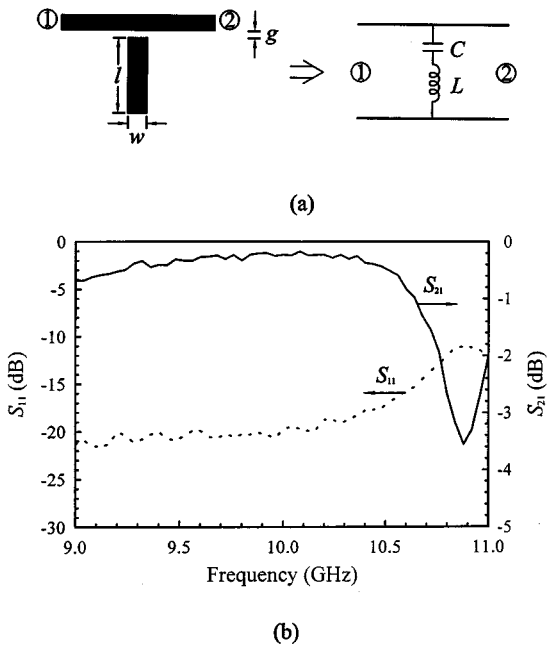

Fig. 4. (a) Configuration and equivalent circuit of the bandstop filter. (b) Measured scattering parameters of a 10.85-GHz bandstop filter with $l = 9.05$ mm, $w = 3$ mm, and $g = 0.1$ mm.

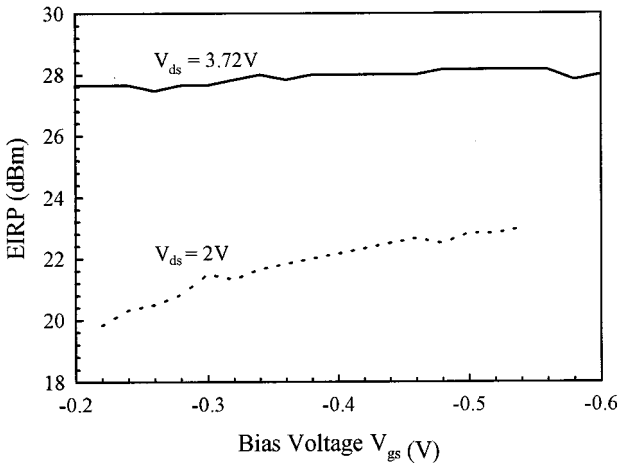

Fig. 5. Variations of the EIRP's as functions of the gate bias $V_{\rm gs}$, for the filter-embedded oscillator with $V_{\rm ds} = 3.72$ and 2 V.

of 10.85 and 9.59 GHz. We were unable to determine which oscillating frequency was generated first. The oscillation depended on the process of changing the drain bias. However, when $V_{\rm ds}$ was further increased near 3.72 V, the oscillating frequency jumped to 10.09 GHz. Further increase of the bias did not change the oscillating frequency. Thus, as predicted in the simulation results, the fabricated four-element antenna oscillator possessed three oscillating frequencies, i.e., 9.59, 10.09, and 10.85 GHz. The deviations of the measured frequencies to the simulated ones are 1.6%,, 0.7%,, and 3.7%, respectively. Fig. 3 illustrates the measured radiation patterns at these frequencies. It is obvious that an in-phase pattern was obtained at 10.09 GHz, which agreed with the corresponding simulation result at 10.02 GHz. Also, as shown in Fig. 2(b), the simulated antenna phase differences at the other two oscillating frequencies are 90° (9.75 GHz) and -90° (10.46 GHz), both corresponding to a radiation pattern with maxima located at $\pm 34^\circ$. Comparing to the experiment results, the radiation patterns at 9.59 and 10.85 GHz, shown in Fig. 3, have the maximum powers appeared at about $\pm 30^\circ$, which are very close to the simulations.

For many applications, an active array with a single stable oscillating frequency and a broadside radiation pattern is needed. To this end, filters with a very narrow stopband may be embedded in the oscillator loop to reject the unwanted oscillating frequencies. These filters should possess a simple geometry to make the design of the whole oscillator compact. Also, they should provide enough attenuation to the unwanted frequencies, while having little influence on the signal propagation at the desired frequency. To fulfill these requirements, the filter structure shown in Fig. 4(a) was used in this investigation. The filter was completed by simply putting an open-ended microstrip stub in the proximity of a microstrip section in the oscillator loop. The stub length l was designed slightly smaller than half of the guided wavelength at the oscillating frequency to be eliminated so that the stub's input impedance was inductive, with the inductance L varying fast near the unwanted frequency. The gap between the stub and microstrip loop section behaved as a capacitor, with the capacitance C depending on the gap length g and the gapwidth (or stub width) w. Thus, the equivalent circuit of this filter was a series *LC* resonator shunted to the microstrip line, as shown in Fig. 4(a). By suitably choosing l, g, and w, the *LC* circuit could be designed to resonate and, thus, be shorted, at the unwanted frequency. Since the stub inductance *L* changes rapidly with the frequency, the stopband of the filter would be very narrow. Fig. 4(b) illustrates the measured scattering parameters for a bandstop filter designed at 10.85 GHz. As is shown, the insertion loss S_{21} of this filter is -3.6 dB at 10.85 GHz, but is only -0.2 dB around 10 GHz. Another filter (with $l = 10.3$ mm, $w = 3$ mm, and $g = 0.1$ mm) has also been designed at 9.59 GHz. The measured results showed an insertion loss of -3.5 dB at 9.59 GHz and -0.3 dB around 10 GHz.

Both the 10.85- and 9.59-GHz bandstop filters were added in the circuit loop. The experiment showed that the original oscillating signals at 10.85 and 9.59 GHz were effectively eliminated. The active array stably oscillated at a frequency around 10.08 GHz when $V_{\rm ds}$ was changed from 2 to 3.72 V, with the radiation beam pointed to the broadside direction. Fig. 5 depicts the variations of the effective isotropic radiation power (EIRP) as functions of the bias voltages. For a fixed gate bias of $V_{\rm gs} = -0.3$ V, when the drain bias was raised from 2 to 3.72 V, the EIRP was enhanced by 6.1 dBm (from 21.5 to 27.6 dBm). However, contrary to these large EIRP variations, the change of the gate bias caused limited variations of the EIRP. For the active devices (i.e., HEMT's) used, at a fixed drain voltage $V_{\rm ds}$, the more negative is the

gate bias $V_{\rm gs}$, the smaller the drain current I_d is and, thus, the lower the dc power ($=V_{\rm ds}I_d$) is consumed. Therefore, the dc-to-RF efficiency can be improved by applying a more negative $V_{\rm gs}$ without disturbing the EIRP significantly.

IV. Conclusions

In this paper, a distributed feedback oscillator with multiple antenna elements has been proposed and implemented at frequencies near 10 GHz. By using the commercial software HP Series IV, the multielement oscillator has been simulated, which showed that the oscillator possessed multiple oscillating frequencies, with each frequency corresponding to a different array radiation pattern. The experiments also confirmed the existence of these frequencies. It was found that the oscillation could be built at one of these oscillating frequencies by changing the biases of the oscillator. For each oscillating frequency, the radiation pattern has also been measured, which agreed very well with the predicted one. In order to attain a single oscillating frequency with a broadside radiation pattern, narrow stopband filters with a simple geometry have been designed and embedded in the oscillator to suppress the unwanted oscillation modes. The measurement verified the efficacy of these filters. For the filter-embedded antenna oscillator, the variation of the EIRP with respect to the change of the bias voltages was measured and compared. The results showed that the increase of the drain bias could effectively raise the EIRP, while that of the gate bias did not change it much. Thus, the dc-to-RF efficiency could be enhanced by using a negative gate bias with a higher voltage. In the future, several multielement antenna oscillators developed in this paper can be suitably arranged into a large active array. By means of the free-space mutual couplings between antennas or external injection signals, the radiated fields from all the oscillators may be coherently combined to create a high output power.

References

[1] J. A. Navarro and K. Chang, *Integrated Active Antennas and Spatial Power Combining*. New York: Wiley, 1996.

[2] B. A. York and Z. B. Popović, *Active and Quasi-Optical Arrays for Solid-State Power Combining*. New York: Wiley, 1997.

[3] Y. Qian and T. Itoh, "Progress in active integrated antennas and their applications," *IEEE Trans. Microwave Theory Tech.*, vol. 46, pp. 1891–1900, Nov. 1998.

[4] J. A. Navarro, F. Lu, and K. Chang, "Active inverted stripline circular patch antennas for spatial power combining," *IEEE Trans. Microwave Theory Tech.*, vol. 41, pp. 1856–1863, Oct. 1993.

[5] J. Birkeland and T. Itoh, "Two-port FET oscillators with applications to active arrays," *IEEE Microwave Guided Wave Lett.*, vol. 1, pp. 112–113, May 1991.

[6] R. D. Martinez and R. C. Compton, "High-efficiency FET/microstrip-patch oscillators," *IEEE Antennas Propagat. Mag.*, vol. 36, pp. 16–19, Feb. 1994.

[7] W.-J. Tseng and S.-J. Chung, "Analysis of a two-port aperture-coupled microstrip antenna," *IEEE Trans. Microwave Theory Tech.*, vol. 46, pp. 530–535, May 1998.

[8] R. A. York, P. Liao, and J. J. Lynch, "Oscillator array dynamics with broadband N-port coupling network," *IEEE Trans. Microwave Theory Tech.*, vol. 42, pp. 2040–2045, Nov. 1994.

[9] J. Birkeland and T. Itoh, "A 16-element quasi-optical FET oscillator power combining array with external injection locking," *IEEE Trans. Microwave Theory Tech.*, vol. 40, pp. 475–481, Mar. 1992.

[10] Y.-C. Yang, S.-J. Chung, and K. Chang, "Novel active antenna amplifying arrays," in *IEEE MTT-S Int. Microwave Symp. Dig.*, Baltimore, MD, June 1998, pp. 997–1000.

Modeling of Broad-Band Traveling-Wave Optical-Intensity Modulators

R. Krähenbühl and W. K. Burns

***Abstract*—In this paper, an accurate simulation tool for the electrical and optical response of broad-band traveling-wave optical intensity modulators is presented, which takes into account multisectional electrical transmission lines. This model is applied to analyze a high-speed fully packaged $LiNbO_3$ Mach–Zehnder interferometer.**

***Index Terms*—Intensity modulator, optical communication, simulation tool, traveling-wave devices.**

I. Introduction

High-speed traveling-wave (TW) broad-band optical intensity modulators are expected to play an important role in future communication systems. Efficient simulation tools are needed to shorten the time of their development, reduce their cost, and to improve their performance in the millimeter-wave frequency spectrum.

Previously, the optical performance of TW modulators have been modeled by considering microwave optical velocity mismatch [1], resistive electrode loss [2], and electrical reflections due to impedance mismatch between electrical connectors and the active device [3]. However, with the advent of fully packaged devices having multisectional electrical transmission lines, considerations such as electrode loss in nonactive sections, reflections from internal impedance transitions, and contributions from discontinuities between the high-frequency connector and electrical line have become very important.

The purpose of this paper is to provide a flexible model for the electrical and optical frequency-domain response of a broad-band TW optical-intensity modulator, by taking into account microwave loss and impedance transitions of the active and any number of nonactive electrical microwave segments. Both the electrical and optical frequency domains are obtained by considering the electrical transmission line as a multisectional microwave cavity. The electrical transmission and reflection responses of the device are directly given by the frequency responses of this microwave cavity. In addition, both amplitude and phase of the microwave-induced optical phase shift are obtained by iterative summation of all co-propagating and counter-propagating electrical waves within the active section of the microwave cavity and direct integration.

II. Microwave-Cavity Model for Optical and Electrical Response

The electrical performances of the microwave electrode in high-speed TW modulators are determined by a complex interplay of device and electrode geometry. This leads to different characteristic impedances and phase velocities in each section along the microwave electrode. To account for several line segments with different electrical characteristics, we treat the electrical transmission line of the modulator as a multisectional microwave cavity. In our considerations and

Manuscript received February 23, 1999. This work was supported by the Office of Naval Research Laboratory.

R. Krähenbühl is with Code 5671, Naval Research Laboratory, Washington, DC 20375 USA, and is also with VPI, Blacksburg, VA 24061 USA (e-mail: roger@ccf.nrl.navy.mil).

W. K. Burns is with Code 5671, Naval Research Laboratory, Washington, DC 20375 USA.

Publisher Item Identifier S 0018-9480(00)03755-8.